Journal of The Electrochemical Society, **154** (8) B835-B844 (2007)
0013-4651/2007/154(8)/B835/10/$20.00 © The Electrochemical Society

Reaction Dynamics in a Parallel Flow Channel PEM Fuel Cell

Jay Benziger,[z] Joanne E. Chia, Erin Kimball, and Ioannis G. Kevrekidis

Department of Chemical Engineering, Princeton University, Princeton, New Jersey 08544, USA

The spatiotemporal dynamic response of a segmented anode parallel channel polymer electrolyte membrane (PEM) fuel cell was monitored following changes in flow rate, temperature and load resistance. Autohumidified operation with dry feeds at 1 bar pressure was achieved at temperatures below 70°C, where the convective transport of water vapor was less than the water production by the fuel cell current. The current could be "ignited" by a single injection of water into the anode feed, or by reducing the temperature and external load resistance. Co-current flow of the hydrogen and oxygen resulted in current ignition at the outlets of the flow channels, followed by a wave of high current density propagating toward the inlets. Counter-current flow of the hydrogen and the oxygen resulted in ignition near the center of the flow channels; over time the ignition front fanned out. The spatio-temporal dynamics of the current ignition along the flow channels can be effectively predicted from a model of a set of coupled differential fuel cells in series. Liquid water condensing in the flow channels gives rise to complex spatio-temporal variations in the current density; these variations are strongly dependent on orientation of the fuel cell with respect to gravity.
 [DOI: 10.1149/1.2745715]

Manuscript submitted October 13, 2006; revised manuscript received April 10, 2007. Available electronically June 15, 2007.

Polymer electrolyte membrane (PEM) fuel cells are complex multiphase chemical reactors, whose principal products are water and an electric current. The basic operation of fuel cells has been reviewed extensively in the literature. Hydrogen and oxygen are fed on opposite sides of an ion-conducting polymer. Hydrogen is oxidized to protons at a catalytic anode and the protons are conducted across the membrane, where they react with oxygen and electrons to make water at a catalytic cathode. The proton current is driven by the chemical potential difference of hydrogen between the anode and cathode. When an external load is connected across the anode and cathode an electron current passes through the external load, matched by a proton current through the ion-conducting membrane. The current is limited by both the external load impedance and the internal resistance of the ion-conducting membrane.

The internal resistance of the polymer electrolyte membrane depends on the water content of the membrane. The water ionizes acid moieties providing mobile protons.[1-4] Nafion, a Teflon/perfluorosulfonic acid copolymer, is the most frequently employed polymer electrolyte; it is chemically robust to oxidation and strongly acidic.[4-6] The electrodes are commonly Pt nanoparticles supported on a nanoporous carbon support and coated onto a microporous carbon cloth or paper. These structures provide high three-phase interface between the electrolyte/catalyst/reactant gas at both the anode and cathode.[7]

There are multiple transport and reaction steps in a fuel cell. PEM fuel cell designs have been heuristically derived to achieve high power output. Many proprietary methods of making membrane-electrode assemblies have been developed, as well as complex patterns of the flow fields, to distribute the reactants to the fuel cell.[5,8,9] There is extensive effort to model PEM fuel cells; models vary in complexity from relatively simple single phase one-dimensional models to complex three-dimensional models that attempt to account for multiphase flow and spatial variations in the water content, current density and reactant concentrations.[3,10-16]

Most fuel cell data is limited to steady state operation. We recently developed the stirred tank reactor (STR) fuel cell to study dynamic operation of PEM fuel cells.[17] The STR PEMFC is a one-dimensional differential cell; longitudinal gradients were minimized, which greatly simplified the analysis of dynamic operation. Ignition/extinction of the fuel cell current and multiple steady states were demonstrated with autohumidified operation resulting from the balance between water production and water removal.[18] ("Current ignition" describes the situation where the steady-state current increases by more than an order of magnitude due to a small change in operating parameter such as the load resistance or reactant flow rate.)

[z] E-mail: benziger@princeton.edu

Almost all large commercial fuel cells employ serpentine flow channels to distribute the gas flow across the active area of the gas diffusion layer.[5,6,14,16,19-21] The flow channels typically have a small cross-sectional area resulting in a high gas velocity that pushes liquid water drops through the flow channels to avoid flooding. As water is a product of the fuel cell reaction, the water concentration increases along the length of the flow channels from the inlet to the outlet.[22] The variable water and reactant concentrations cause the current density to vary throughout the fuel cell. Interpreting the integrated current density and average voltage to changes in feed flow rates and load becomes intricate with the serpentine flow channels.

To help identify the essential physics that should be included in PEM fuel cell modeling efforts, we developed a segmented anode parallel channel (SAPC) fuel cell reactor. The SAPC PEM fuel cell reactor has a simplified two-dimensional geometry. It can be easily modeled by a number of STR PEM fuel cell reactors in series that simplify the analysis of the dynamic operation. We present here data for autohumidified operation of the two-dimensional reactor demonstrating current ignition and reaction front propagation along the flow channels. Flow configurations impact the location of the initial current ignition in the flow channel and the direction of propagation. We show that large current fluctuations occur between different segments along the flow channel that appear to be correlated with water droplet motion. Finally, we show the importance of gravity on liquid water flow in the gas flow channels.

The Segmented Anode Parallel Channel PEM Fuel Cell

To examine the current distribution along a PEM fuel cell flow channel, a two-dimensional fuel cell with parallel flow channels at the anode and cathode and a segmented anode was constructed; we refer to this reactor as the segmented anode parallel channel (SAPC) fuel cell. Local current densities were measured through each anode segment; the cathode was fabricated as a single unit. The membrane electrode assembly (MEA) was also fabricated as a single assembly. The reactor was designed with the lateral separation between anode segments >10 times the transverse separation between the anode and cathode, so that the transverse current is large compared to the lateral currents.

We have built two versions of SAPC fuel cells. Version one had three parallel flow channels at both the anode and cathode. The cathode was a machined block of graphite with three parallel flow channels $2 \times 2 \times 30$ mm long. The entire graphite block was press fit into a larger piece of Teflon for electrical isolation. The flow channels initiated and terminated in common manifolds in the Teflon block at both ends of the graphite flow channels. The anode had the same channel structure, except that it was made of six graphite pieces separated by Teflon spacers inserted into a Teflon block. Copper foils were pressed against the graphite plates and copper wires

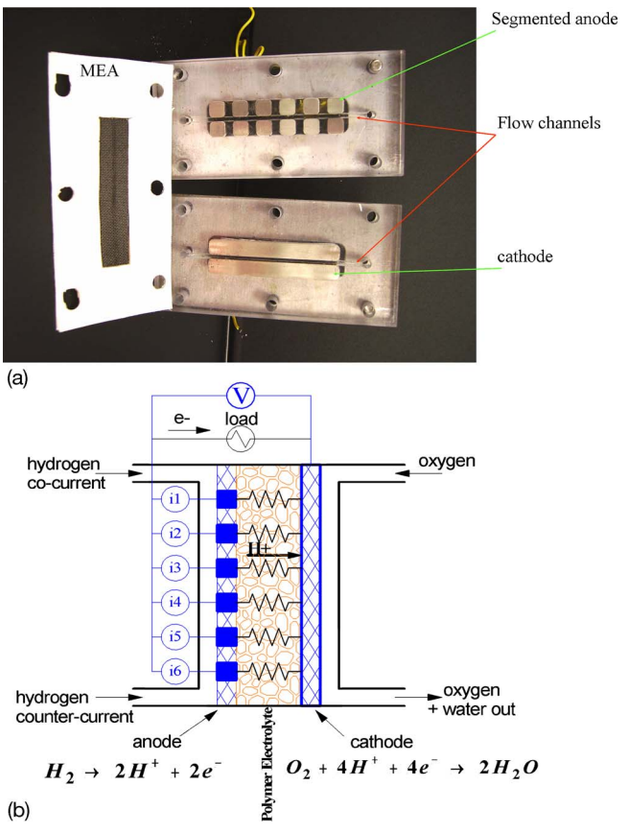

Figure 1. (Color online) (a) Segmented anode fuel cell. The flow channels and divisions of the anode are shown. The basic setup for temperature control, reactant feed, and relative humidity and water flow measurements for the segmented anode fuel cell was the same as the one employed with the differential PEM fuel cell.[17] (b) Equivalent circuit for the segmented anode fuel cell. The current through each segment as well as the voltage drop across the load resistance were monitored. The voltage across the load resistance was recorded as well as the currents through the six segments of the anode. The total current was determined by summing the individual currents through the six segments of the anode.

were attached to connect them to the external load resistor. Each of the graphite segments was connected individually to a lead wire and run through a 0.1 Ω sensing resistor.

After a series of experiments with the first SAPC, we built a second version with a single flow channel at both the anode and cathode. The flow channels were 1.6 mm wide × 3.2 mm deep × 75 mm long, machined out of polycarbonate. The cathode consisted of two stainless steel pieces 6.4 mm wide × 54 mm long, that lined both sides of the flow channel as seen in Fig. 1a. A threaded rod was connected through the polycarbonate plate into the stainless steel pieces. The anode had twelve stainless steel pieces, 6.4 mm square, machined to fit into a polycarbonate plate separated by 3.2 mm along the channel delineating the flow channel. Copper wires were soldered to the stainless steel leads from the electrodes. The stainless steel segments straddling the flow channel from each other were jumpered together to form a single anode segment. The lead wires from each anode segment were connected individually to a 0.1 Ω sensing resistor, R_{sense}. With external illumination it was possible to see the MEA in the flow channel through the polycarbonate.

The six leads from sensing resistors at the anode were connected together, and the common lead was connected through a 0–20 Ω 10-turn potentiometer to the cathode. The entire assembly was mounted between two aluminum blocks that were temperature controlled using cartridge heaters. A computer DAQ board read the voltage drop across the potentiometer (that served as the load resistance) and the voltage drop across each of the sensing resistors. The currents through each of the six segments of the anode were determined by multiplying the voltage drop across the sensing resistors by 10 $(1/R_{sense})$. The electrical equivalent of the segmented anode fuel cell is shown in Fig. 1b.

An MEA was placed between the cathode and anode and sealed. We made our own MEA of a Nafion 115 membrane pressed between 2 E-TEK electrodes (these consist of a carbon cloth coated on one side with a Pt/C catalyst). The catalyst weight loading was 0.4 mg-Pt/cm^2. The electrodes were brushed with solubilized Nafion solution to a loading of ~1 mg-Nafion/cm^2 before placing the membrane between them.[23] The assembly was hot pressed at 130°C and 10 MPa. The Nafion membrane extended beyond the carbon cloth by ~3 mm and was pressed between silicon rubber sheet gaskets that sealed the MEA from the sides. The MEA in the single channel fuel cell (Version 2) was 12 mm wide and 75 mm long.

Hydrogen and oxygen were supplied from commercial cylinders through mass flow controllers at flow rates, F = 1–20 cm^3/min (sccm). The effluents were bled into 10 mL graduated cylinders with a small hydrostatic head (~2 cm H_2O), so that the cell pressure was effectively 1 bar. The water in the graduated cylinders also kept air from back diffusing into the flow channels. The flows at the anode and cathode could be either co-current or counter-current. The fuel cell could be oriented with the flow channels either vertical or horizontal; we see below, the orientation of the flow channels has a dramatic effect on the fuel cell operation.

Tees with relative humidity sensors (Honeywell 3610) were positioned at the outlets from both the anode and cathode to measure the water activity in the effluents. A tee with a septum was placed at the inlet to the anode. This permitted direct injection of fixed aliquots of water to the anode.

Dynamics of Start-up of a PEM Fuel Cell

The membrane water content must be sufficient for a PEM fuel cell to sustain an acceptable current density. Can the fuel cell make enough water to keep the fuel cell functioning? Autohumidified fuel cell operation employs dry feeds; the water to humidify the electrolyte membrane is provided by the fuel cell reaction.[24-26] Two conditions must be satisfied for autohumidified operation of a fuel cell: water production must be sufficient to balance water removal, and there must be sufficient water present in the membrane initially to ignite the fuel cell current.[27] A dry membrane will have a large resistance and limit the fuel cell current, making it very small. Alternatively, if the external load being driven by the fuel cell is increased, it will reduce the current so that less water is produced; this will cause the membrane to dry and extinguish the current. The two-dimensional fuel cell with flow channels results in lateral gradients in composition and current density. The local water balance along the length of the flow channels is controlled by the local current density, convective flow in the gas flow channels, and diffusion of water in the membrane. Ignition and extinction of the fuel cell current along the flow channels in a PEM fuel cell with dry feeds (autohumidified operation) are presented below.

Ignition and extinction in co-current flow.— The initial water content in the polymer electrolyte membrane was set to a "dry state" before starting an experiment. The dry state was defined such that the current through each segment in the fuel cell was <1 mA when the fuel cell load was shorted out ($R_L < 0.5$ Ω). Initially, we prepared a dry state at 80°C. The polymer membrane was dried by flowing dry oxygen through the cathode chamber at 10 sccm and dry hydrogen through the anode chamber at 10 sccm for ~12 h at 80°C with the fuel cell at open circuit. With a dry membrane, a finite load resistance of 0.2–20 Ω could be connected between the anode and cathode and the fuel cell and the current through each anode segment circuit was negligible (<1 mA). We subsequently discovered that the "dry" state could be achieved by passing dry gases

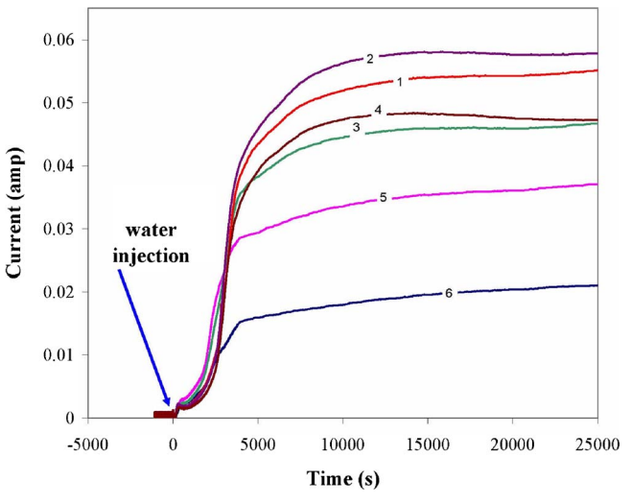

Figure 2. (Color online) Ignition of the SAPC fuel cell by water injection. Co-current flow of reactants at 25°C with a load of 0.5 Ω. 50 μL of water were injected into the anode feed stream at $t = 0$. (Data file name: MEA2-25C-constco-startup2)

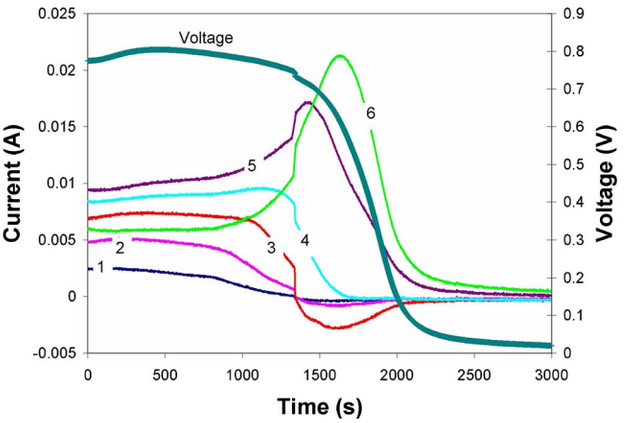

Figure 3. (Color online) Fuel cell extinction at 80°C. The reactant flows were co-current. At $t = 0$ the load resistance was increased from 0.5 to 20 Ω. The currents are designated by segment number. The voltage is the voltage drop across the load impedance. (Data file name: MEA2-80C-constco-extinguish6)

through the fuel cell at 25°C and open circuit for 16 h. A fuel cell in the "dry" state had "zero" current through each segment of the fuel cell with a small load resistance ($R_L < 0.5$ Ω) and dry feeds.

Once the membrane was dry, the set point on the temperature controller was adjusted. After the fuel cell temperature stabilized, the external load resistance was set, the reactant flow was started, and data collection was initiated. Temperature, relative humidity in the anode and cathode effluents, voltage drop across the load resistance, and the current through each anode segment were automatically logged every 1–100 s (the frequency was varied depending on the specific experiment, with the concern to keep the files manageable for data processing).

With a "dry" membrane and fuel cell temperature ≥60°C the SAPC fuel cell current was always negligible (<1 mA total current), even when the external load resistance was shorted out. The fuel cell current was ignited by first shorting out the external load ($R_L < 0.5$ Ω) and then either reducing the temperature or injecting an aliquot of liquid water into the anode feed. Figure 2 shows the current ignition at 25°C following water injection. (Data file names are listed with the figure. These data files are posted as supplemental information available at our web site.) The fuel cell was positioned with the flow channels running vertically and the flows running co-current from top to bottom. Segment 1 is at the inlet for the anode and cathode. The fuel cell current was near zero with a load resistance of 0.5 Ω and flow rates of 3 sccm H_2 at the anode and 1.5 sccm O_2 at the cathode. At time zero, 50 μL of liquid water were injected into the anode feed. About 150 s after the water injection, the current in each segment increased to ~3 mA. 1500 s after the water injection, the current began to rise rapidly approaching steady state around 3000 s after the water injection and increased to steady state currents between 20–50 mA in each segment. The steady state currents are highest near the inlet and fall off toward the outlets of the flow channels.

The fuel cell current will only stay ignited as long as the water produced is greater than or equal to the water removed by convection in the effluents. Water removal scales with the vapor pressure of water, hence it increases with temperature. Water production scales with the current, hence it decreases with increasing load resistance. Increasing the temperature and increasing the load resistance can cause the fuel cell current to extinguish. Figure 3 is an example of extinction of the fuel cell current by increasing the load resistance. An ignited SAPC fuel cell was operated at 80°C with flow rates of 6 sccm H_2 at the anode and 3 sccm O_2 at the cathode and a load resistance of 0.5 Ω. The fuel cell was operated with co-current flow and was positioned vertically with the feeds entering at the top at segment 1. At time zero, the load resistance was increased to 20 Ω. Approximately 1000 s after increasing the load, the current in segment 1 began to drop to zero. The current in the other segments extinguished sequentially from the inlet (segment 1) to the outlet (segment 6) as the membrane dried out. Two unusual features of the extinction of the fuel cell current are evident in Fig. 3. The first is that in segments 4, 5, and 6 the current increased before extinguishing. This is attributed to proton currents moving upstream on the cathode after the anode segments were extinguished. Second, the currents in segments 2 and 3 went negative while the currents rose in segments 4, 5, and 6. This is attributed to local potential differences driving internal currents. The voltage across the load resistance is also plotted in Fig. 3. The voltage stays almost constant until the current in segment 6 of the fuel cell starts to extinguish, and then the voltage drops to zero as the current through the load falls to zero. When the membrane is dry, most of the potential drop occurs across the membrane and there is negligible voltage drop across the load. However, as long as any one segment remained ignited, the voltage drop across the load was almost independent of the active area of the membrane-electrode-assembly.

Extinction of the fuel cell current depends on a balance of the water production and water removal. When the flow rates of hydrogen and oxygen were reduced from 6 and 3 sccm, respectively, to 3 and 1.5 sccm, the time for the current extinction was 4000 s; it took twice as long for the current to extinguish when the flow rate was halved. Alternatively, it was observed that when the load resistance was increased to 10 Ω instead of 20 Ω, the time for current extinction was 2500 s; it took longer for the current to extinguish when the load resistance was halved because the water production rate was greater. There is a critical load resistance below which the current will not extinguish; it is a function of both temperature and flow rate, but we did not attempt to determine that condition experimentally.

After the fuel cell current is extinguished, the current can be reignited by reducing the load resistance and reducing the temperature. Reducing the fuel cell temperature reduces the water removed by convection. The flows to the anode and cathode were shut off after the fuel cell was extinguished and the temperature controller was reset from 80 to 25°C. By stopping the gas flow through the fuel cell the membrane was "dry" from the viewpoint of its resistivity being large enough to limit the current to <1 mA, but the membrane was not dried to where the resistivity became excessively high and limited the current to ~1 μA. Once the temperature was at

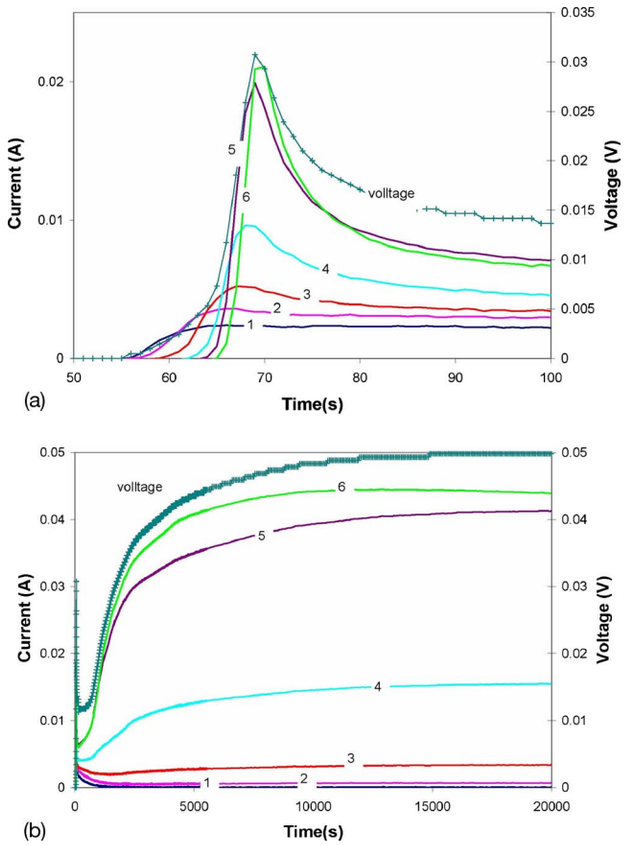

Figure 4. (Color online) (a) First 100 s of reignition of the SAPC fuel cell after extinction. Temperature was 25°C; load resistance was 0.5 Ω. The currents are designated by segment number. The voltage is the voltage drop across the load impedance. At $t = 0$ the reactant flows were started at 6 sccm H_2 and 3 sccm O_2. (Data file name: MEA2-25C-constco-startup4). (b) The complete reignition of the SAPC fuel cell after extinction. The first ignition point is when hydrogen first flows into the flow channel; the second ignition corresponds to rehydration of the membrane.

25°C, the load resistance was reduced to 0.5 Ω and the flow to the fuel cell was started up at 6 sccm H_2 at the anode and 3 sccm O_2 at the cathode. The fuel cell was in a vertical orientation with the feeds entering at segment 1. The dynamic response during the start-up is shown in Fig. 4a and b. Figure 4a shows the first 100 s after the flow was started, and Fig. 4b shows the response over 10,000 s.

Figure 4a and b show a two-step current ignition. The first current ignition started 50 s after the flow started with a small current of 3 mA in segment 1, and then each segment ignited in sequence over a period of 10 s. The first ignition step shows a peak in the current that lasts for ~10 s after which the current and voltage both decrease to a low value. This first ignition step occurred when the hydrogen and oxygen flows first reached the membrane-electrode interface. The first reaction front moves along the channel at ~1 cm/s. The gas velocity in the flow channels is ~10 cm/s. The first current front propagates slower than the gas velocity because of gas diffusion across the gas diffusion layers in the MEA. The second ignition step, depicted in Fig. 4b, begins after 1000 s and takes a period of ~500 s for the currents to reach a steady state. The second ignition step is different from the first ignition step. The second ignition step shows the currents rising to a high value and remaining at those high values. The currents in segments 5 and 6 are the first to ignite in the second stage of ignition, followed by segment 4. Segments 1 and 2 appear to extinguish and segment 3 sustains only a small current. The voltage across the load resistance rises coincidentally with both ignition steps. The second ignition step is ascribed to hydration of the membrane by the water produced in the fuel cell.

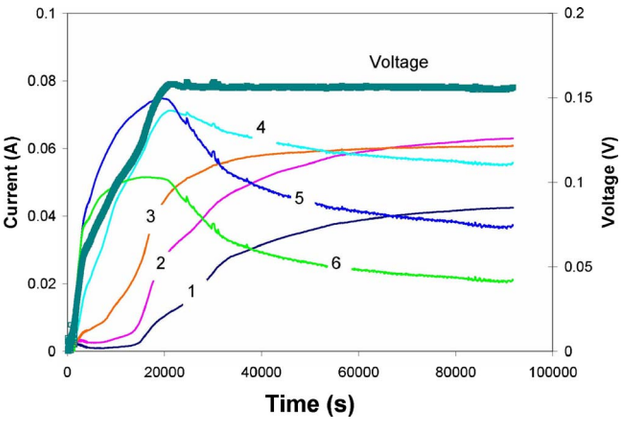

Figure 5. (Color online) Reignition of the SAPC fuel cell after extinction. Flow is co-current downward with inlets at segment 1. Temperature was 25°C; load resistance was 0.5 Ω. The currents are designated by segment number. The voltage is the voltage drop across the load impedance. At $t = 0$ the reactant flows were started at 3 sccm H_2 and 1.5 sccm O_2. (Data file name: MEA2-25C-constco-startup)

Figure 5 shows a different ignition experiment with all the conditions the same as those used for Fig. 4 except that the flow rates were reduced to 3 sccm H_2 and 1.5 sccm O_2 at the anode and cathode. Reducing the flow rates reduced the convective transport of water. Diffusion of water in the membrane can then propagate upstream against the convective flow. This resulted in the current ignition of segments 3, 2, and 1 of the SAPC fuel cell. A comparison of Fig. 4b and 5 are illustrative of how the balance between convection and diffusion can dramatically alter the current distribution in PEM fuel cells.

Ignition and extinction in counter-current flow.— The inlets at the anode and cathode can be configured so the gas flow is counter-current. The SAPC fuel cell was set up with the flow channels running vertically and hydrogen and oxygen flows running counter-current. For the results presented here the oxygen flow at the cathode was running from top to bottom and the hydrogen flow ran from bottom to top. (We anticipated more liquid would form at the cathode, so the configuration was arranged to remove liquid by

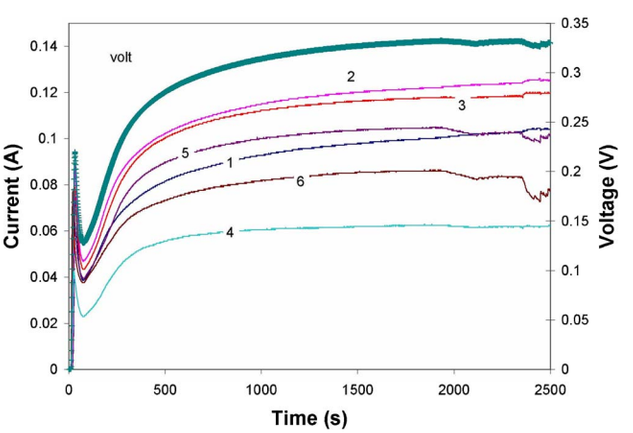

Figure 6. (Color online) Current ignition in counter-current flow. Hydrogen inlet is a segment 6 and oxygen inlet is at segment 1. The currents are designated by segment number. The voltage is the voltage drop across the load impedance. Temperature is 25°C with inlet flow rates of 6 sccm H_2 and 3 sccm O_2. (Data file name: MEA3-25-constcnt-startup)

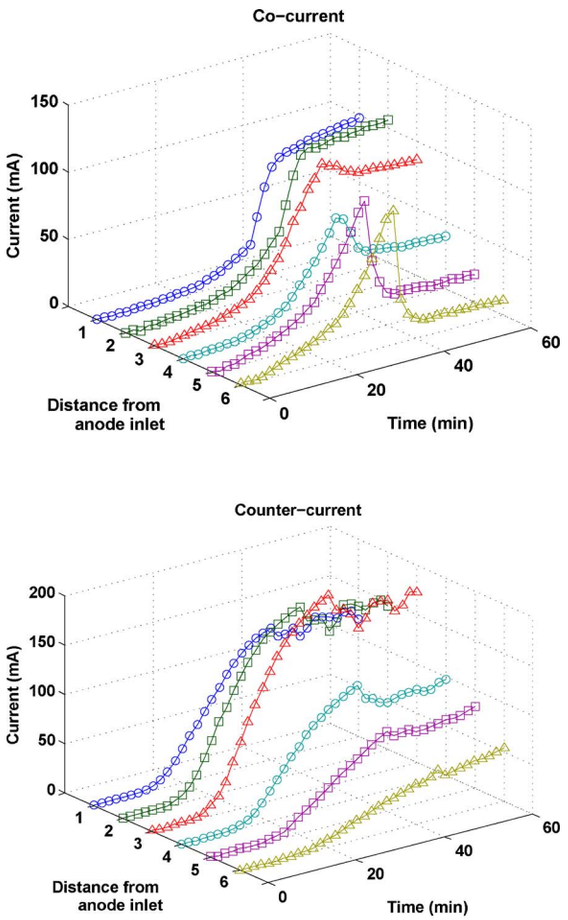

Figure 7. (Color online) Proton current ignition fronts in co-current and counter-current flow. The current in each segment (in mA) is shown as a function of time. Time is recorded from the start of flow after cooling down the fuel cell. The 3-D graph to the left is for co-current flows at the anode and cathode; the one to the right is for counter-current flows at the anode and cathode.

gravity at the cathode.) Figure 6 shows the ignition of the SAPC fuel cell with counter-current flows. The fuel cell was first extinguished by operating with dry feeds at 80°C with a load resistance of 20 Ω. The flows were stopped, the fuel cell cooled down to 25°C, and the load resistance set to 0.5 Ω. After the temperature had equilibrated at 25°C the flows were initiated: 6 sccm H_2: the anode and 3 sccm O_2 at the cathode. Counter-current flow produced a different ignition pattern than co-current flow. Ignition occurred near the center of the flow channel. And, after ignition, a current front fanned out in both directions with the all segments igniting over a period of ~100 s. A simple visual comparison of Fig. 5 and 6 shows that ignition occurred over a much shorter time period with counter-current flow as compared to co-current flow.

The difference between co-current and counter-current flow is shown in Fig. 7, which is a 3-D plot of the local current density as a function of time. Co-current reactant flow ignites the proton current at the outlet of the flow channels; after ignition the proton current ignition front propagates towards the inlet of the flow channel. As the proton ignition front propagates upstream, the current drops off in the downstream section of the flow channel. In contrast, counter-current flow shows that the proton current ignition near the center of the flow channel, with the proton current front fanning out from there.

Extinction of the proton current with co-current flow was the

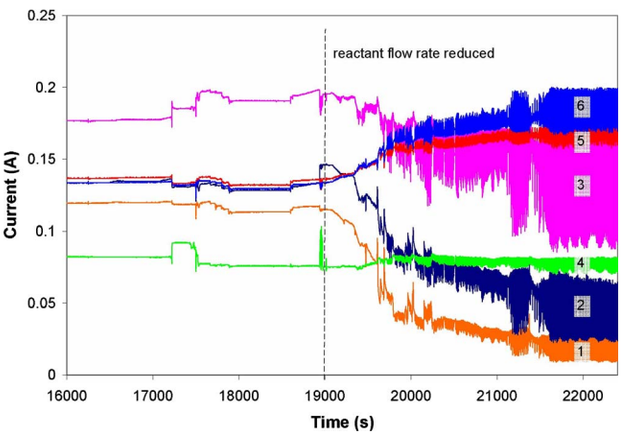

Figure 8. (Color online) Current distribution in the SAPC fuel cell with co-current flow upward. The flows enter at segment 6 and exit at segment 1. The fuel cell temperature was 25°C; load resistance was 0.5 Ω. The currents are designated by segment number. The voltage is the voltage drop across the load impedance. At $t < 19000$ s the flow rates were 12 sccm H_2 and 6 sccm O_2; at $t > 19000$ s the reactant flows were reduced to 6 sccm H_2 and 3 sccm O_2. (Data file name: MEA3-25-constco-startup12)

reverse of ignition. Increasing the load resistance under co-current flow conditions resulted in proton current extinction starting at the inlet, and the proton current front extinction front propagated to the outlet. When the load resistance was increased with counter-current flow, the proton current extinguished from both ends, narrowing the ignition band to a region in the center of the flow channel until the fuel cell proton current finally extinguishes.

Effect of gravity on current stability.— The results in Fig. 2-5 were obtained with the gas flows at the anode and cathode being co-current downward in the direction of gravity. At 25°C, sufficient water is formed that liquid water can condense in the flow channels, especially the cathode flow channel. When the gas flow is in the same direction as gravity, any liquid water formed in the fuel cell is swept out by the gas flow. When we performed experiments with counter-current gas flows, shown in Fig. 6 and 7, we had the cathode flow going downward. Because most of the liquid water product ends up at the cathode, the gas flow at the cathode swept out almost all the liquid water formed. In all of the experiments conducted with gas flow downward, the steady state proton current was stable; there was little fluctuation of the proton current, independent of the inlet gas flow rates.

When the gas flow at the cathode was upward, against gravity, we saw that the stability of the proton current depended on the gas flow rates. There were no significant differences in the proton current evolution during ignition of the fuel cell from a dry state between upward and downward gas flows. However, after ignition, when liquid water began to accumulate in the flow channels, the flow direction relative to gravity made an enormous difference. Figure 8 shows the proton current distribution when the gas flow rates were reduced at 19000 s from 12 sccm H_2 and 6 sccm O_2 to 6 sccm H_2 and 3 sccm O_2. The gas flow in Fig. 8 enters at segment 6 and exits at segment 1. When the gas flow at the cathode was in the direction of gravity the proton currents became steady after ~4000 s, independent of flow rate (see Fig. 4b and 5). However, when the flow was flipped so that the cathode gas flow opposed gravity, entering at the bottom and exiting at the top of the flow channels, the proton currents in the ignited section of the fuel cell were stable at the higher gas flow rates and then showed large fluctuations at the lower gas flow rate.

Figure 8 shows that when the inlet reactant gas flow rates were reduced, the average proton currents increased in the anode segments near the inlet. As the gas flow rate is reduced, water diffusion

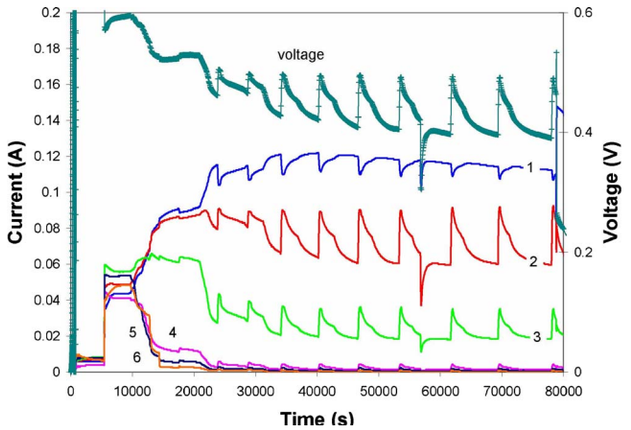

Figure 9. (Color online) SAPC operated with counter-current flows in a horizontal configuration. The initial flow rates were 10 sccm H_2 and 10 sccm O_2; at t = 5500 s the load resistance was reduced from 18 to 2 Ω, resulting in ignition of the fuel cell current. The currents are designated by segment number. The voltage is the voltage drop across the load impedance. The fuel cell temperature was 25°C. At 21000 s the flow rates were reduced to 6 sccm H_2 at the anode and 3 sccm O_2 at the cathode. (Data file name: retesting.xls)

in the membrane becomes more significant relative to water convection, resulting in increased membrane hydration near the inlets. The same phenomenon was also seen in Fig. 4b and 5 when the gas flow was downward.

The fluctuations in the proton current seen in Fig. 8 are attributed to slugs of liquid water in the flow channels that had to be pushed against gravity by the gas flow. We were able to see the water slugs in the cathode flow channel in the SAPC fuel cell constructed with polycarbonate. With the inlet oxygen flow rate of 6 sccm water slugs formed every 10 s and were swept through the flow channel in ~3 s. The liquid slugs appeared to move at the velocity of the gas, and the water slugs exited the flow channel before the next slug formed. When the gas flow rate was reduced, a second liquid water slug was formed in the channel before the first slug exited the channel. When more than a single liquid water slug was in the cathode flow channel, it affected the oxygen concentrations upstream of the slug, causing the current to fluctuate.

With counter-current flow, either the anode or cathode gas flow will be in the direction of gravity. When the cathode flow was in the direction of gravity we did not see any significant current fluctuations and the SAPC fuel cell operation was similar to that seen with co-current flow downward. However, when the cathode flow was upward, against gravity, we saw qualitatively similar performance to that shown in Fig. 8. The results indicate that more liquid is accumulated in the cathode flow channel.

Horizontal fuel cell orientation.— The SAPC fuel cell was operated with the flow channels running horizontally and with the flows running co-current and the inlets at segment 1. Ignition of the fuel cell proton current follows the same sequence for co-current flows for both horizontal and vertical orientations. Proton current ignition with counter-current flows was also the same for both horizontal and vertical orientations. When the fuel cell is horizontal and liquid water slugs form, they cause the proton current to fluctuate, but the fluctuations are different than those shown in Fig. 8 for the vertical orientation. Figure 9 shows the operation of the SAPC in the horizontal orientation with counter-current flow. The fuel cell current ignited and after ignition the currents in each segment were approximately equal for ~8000 s. After 8000 s, approximately 0.4 cm^3 equivalent of liquid water has formed, comparable to the volume of the flow channel (0.375 cm^3). Because the vapor pressure of water is low at 25°C (0.025 bar) most of the water remains as condensed liquid in the flow channel. The liquid water forms a plug that gets

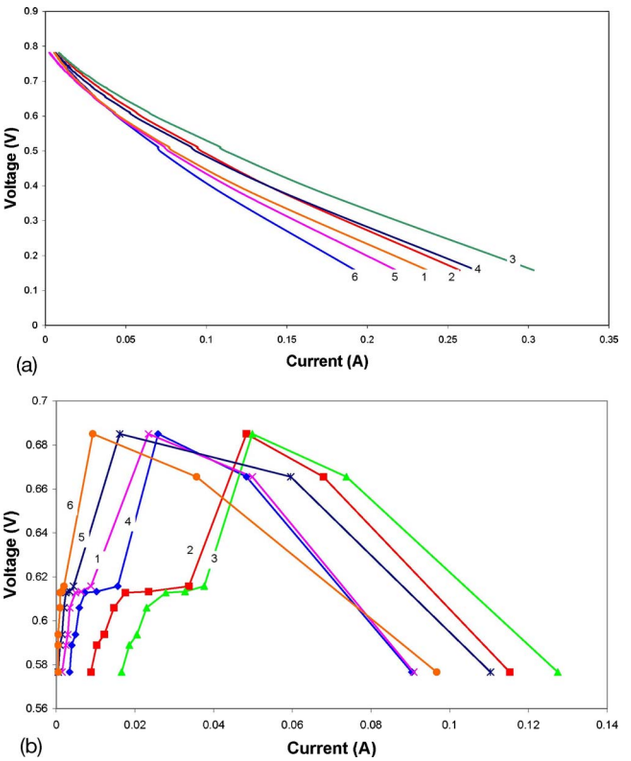

Figure 10. (Color online) (a) "Instantaneous" polarization curve for the SAPC fuel cell after ignition. This was obtained by sweeping the external load from 0.2 to 20 Ω in ~100 s. This sweep was taken for the counter-current flow shown in Fig. 8 1500 s after ignition. (Data file name: retesting2.xls) (b) "Steady state" polarization curves for the SAPC fuel cell. The steady state current and voltage were obtained by stabilizing the fuel cell for ~5000 s at fixed load resistance. The load resistance was increased stepwise by 2 Ω over the range 2–20 Ω. (Data file name: retesting2.xls)

pushed downstream, flooding the cathode flow channel at segments 4–6. As more water is formed, slugs accumulate that block part of the upstream flow channel causing the current to drop. As the current drops, the gas pressure builds up until it eventually pushes forward pushing a slug of water out of the flow channel. The motion of the water plug can be followed by the rise and fall of currents in each segment as the water droplets go past. This problem was not observed when the fuel cell was in the vertical orientation and gas flow going in the direction of gravity. When the gas flow was downward, the water droplets fell to the bottom of the flow channel and were swept out of the flow channel.

Local polarization curves.— The most common characterization of fuel cells is the current-voltage response, commonly referred to as the polarization curve. The polarization curve is obtained by measuring the current through and the voltage across the external load resistance as the load resistance is varied. In the intermediate current range the slope of the polarization curve is approximately equal to the negative of the membrane-electrolyte resistance. With the SAPC fuel cell we can obtain local polarization curves associated with each segment of the anode.

Figure 10a shows the "instantaneous" polarization curves for the SAPC fuel cell operating counter-currently. The fuel cell was equilibrated at 25°C and with flow rates of 6 sccm H_2 at the anode and 3 sccm O_2 at the cathode and a load resistance of 0.5 Ω. To obtain the "instantaneous" polarization curve the external load resistance was swept from 0–20 Ω over a period of ~100 s. By completing the sweep in a short time, the water content in the fuel cell remains nearly constant; the total water production and water removal are both small over 100 s relative to the total water inventory in the fuel

cell. The slopes of the polarization curves match our intuitive assumptions about the water content in the membrane; the lowest resistances are in segments 3, 4, and 2, near the center of the flow channel, while the resistances are higher at the inlets because of drying from the feed streams. The resistances vary from 1.5 Ω in segment 3 to 2.8 Ω in segment 6.

Figure 10b shows the "steady state" polarization curves for the SAPC fuel cell operating autohumidified with counter-current flows at 25°C and with flow rates of 8 sccm H_2 at the anode and 4 sccm O_2 at the cathode. Starting with a load resistance of 2 Ω, the current and voltage were recorded as a function of time. The resistance was increased by 2 Ω every 2 h, and we plotted the steady state current and voltage after 2 h. The most obvious difference between the instantaneous and steady state polarization curves is that at low currents the voltage on the steady state polarization curves drop as the fuel cell membrane dehydrates. From Fig. 10b, we can identify the critical load resistance of 6 Ω for autohumidified operation at the specified conditions of temperature, flow rate, and flow configuration. At lower loads the fuel cell will sustain autohumidified operation indefinitely. At loads >6 Ω the fuel cell current will begin to extinguish as water removal by convection exceeds water production.

Discussion

We previously reported the existence of ignition/extinction phenomena in an STR PEM fuel cell.[17,24,25] The fuel cell current ignited when the water production in the fuel cell exceeded the water removed by convection. Current ignition in a PEM fuel cell results from the positive feedback between the membrane resistivity and the water produced in the fuel cell. The membrane resistivity decreases exponentially with increasing water activity,[28] consequently the water production increases exponentially with water activity (a_w), while the water removal increases linearly with water activity. This gives rise to steady state multiplicity and critical water activity for current ignition. This is analogous to thermal ignition in an STR with an exothermic reaction.[29-31] The critical water activity for ignition is analogous to the critical temperature for ignition with an exothermic reaction in an STR.

In this paper, we have shown how the concepts of ignition and extinction can be extended to spatio-temporal reaction front propagation which is controlled by flow rate, temperature and load resistance. Qualitatively, we can describe how these parameters control ignition.

Increasing the flow rate dilutes the concentration of water in the gas streams, reducing the total amount of water that is absorbed into the membrane. Only at low flow rates, when the gas streams are sufficiently humidified by the water formed upstream, will the fuel cell ignite.

Increasing the temperature increases the vapor pressure of water. For the same amount of water formed, less water is retained in the membrane at higher temperature; this dries out the membrane and extinguishes the fuel cell.

Increasing the load resistance reduces the current through the fuel cell circuit and, hence, decreases the water production. With less water formed, the water activity decreases and, hence, the fuel cell extinguishes.

The STR is a one-dimensional reactor, with the gradients only transverse across the membrane. Larger area PEM fuel cells must distribute the reactants over a large area, generally involving complex flow channel arrangements.[5,8,21] The gas distribution system will result in lateral gradients of water concentration and variations in gas velocity.[22,32] The SAPC is the simplest two-dimensional fuel cell system we can envision; it permits the study of lateral gradients and transport on fuel cell performance in a simple and well-defined geometry.

The SAPC fuel cell offers significant advantages to conventional PEM fuel cells for the study of fuel cell dynamics. There have been several numerical studies to predict dynamics of the current distributions in PEM fuel cells.[33-36] These models have made predictions about the role of in-plane water diffusion in affecting the local current distributions in PEM fuel cells. These models and others have not had direct verification because there have been no reports of the dynamics of current distributions in PEM fuel cells. The results presented here are the first experimental results showing the temporal evolution of the current distribution in a 2-D fuel cell.

Ignition and extinction front propagation can be understood by considering the connection between the local water content in the membrane and the local current density (which is proportional to water production), water convection by gas flow in the flow channels and water diffusion in the membrane. When the flows are co-current, ignition occurs at the outlet of the flow channels because the water produced in the fuel cell is convected downstream and accumulates fastest at the outlet. Provided that the temperature and flow rates are sufficiently low, the water can accumulate until the resistance in the membrane drops sufficiently for the current to ignite. After ignition, the water concentration increases in the downstream sections of the membrane, which drives water diffusion upstream through the membrane. The movement of the current ignition front results from a balance between the water transport downstream by convection in the flow channel and water transport upstream by diffusion in the membrane. Reducing the flow rates in the flow channel will cause the front to propagate even further upstream, as seen in comparing Fig. 4b and 5.

Extinction of co-current flow is a result of the drying of the membrane by convection, when the current is too low to sustain the water in the membrane. Drying is enhanced at higher temperature, higher load resistance, and higher flow rates. Drying proceeds from the inlet toward the outlet as water evaporates from the membrane into the gas flowing in the flow channels.

Counter-current flow produces a different ignition pattern than co-current flow because water is convected in opposite directions in the anode and cathode flow channels. This results in water accumulating fastest at an interior position along the flow channel, a location determined by the relative flow rates at the anode and cathode. When the flow rates were nearly equal, we saw that the ignition was close to the center of the cell. Altering the flow rates pushes the ignition point downstream in the direction of the higher flow. The fanning of the ignition front in counter-current flow results from water diffusion in the membrane in both directions away from the highest concentration, the ignition point.

The qualitative experimental trends of the sequence of current ignition and extinction along the length of the flow channel follow our expectations. However, the steady state current profiles were not identical to what we expected. The steady state current profiles were affected by nonuniformities in the membrane electrode assembly caused by variations in compression. These variations altered the local resistances associated with the segmented electrode. We suspect that unitary assembly of commercial MEAs would show better uniformity than we report here. Our concern here is to identify the generic fuel cell pathology that will be exhibited by PEM fuel cells, and we want to focus on that generic behavior.

We can get a semiquantitative match to the ignition/extinction behavior in the segmented anode parallel channel fuel cell with a relatively simple model. Our STR model can be extended to a "tanks-in-series" model, treating each segment of the anode as a differential reactor.[37-39] The dynamic time scales for the ignition and front propagation are dictated by water sorption in the membrane, the convective flow rates in the anode and cathode channels, and the diffusion rate of water in the membrane.

Water sorbs into the polymer, ionizing sulfonic acid groups facilitating proton transport; water sorption scales with the number of sulfonic acid groups in the membrane and the proton conductivity depends on the sulfonic acid density (N_{SO3}) and the number of water molecules hydrating each sulfonic acid (λ). Water is sorbed into the membrane when the water activity in the gas flow channels is greater than the water activity in the membrane, and water desorbs when the water activity is greater in the membrane. We make the simplifying assumption that the water activity in the membrane is in

local equilibrium with the water activity in the gas flow channels, and the only gradients are longitudinal along the channel. With the STR PEM fuel cell, we found that water activity in the anode and cathode gas flow channels are nearly equilibrated with the membrane for current densities <1 A/cm^2.[18,25]

The water balance in each differential element of the membrane is given by Eq. 1 ($j = 1$–6; $j = 0$ is the feed and because water cannot diffuse from outside the fuel cell $a_{w7} = 0$). The water inventory is the balance between water produced (one-half the proton current), water convected in the gas flow, and longitudinal water diffusion (described by a lumped mass transfer coefficient between differential elements). The water inventory includes water in the membrane and water vapor in the flow channels; in general, the water vapor in the flow channels is much less than water sorbed in the membrane, in which case the second term on the left hand side of Eq. 1 can be ignored. Equation 2 is an empirical fit to the number of water molecules associated with each sulfonic acid group as a function of water activity in a Nafion 115 membrane[28,39]

$$\left(N_{SO_3}\frac{d\lambda_{(j)}}{da_{w(j)}} + \frac{(V_A + V_C)P^o_w}{RT}\right)\frac{da_{w(j)}}{dt} = \frac{i_{(j)}}{2F} + (F_{A(j-1)} + F_{C(j-1)})\frac{a_{w(j-1)}P^o_w}{P_T} - (F_{A(j)} + F_{C(j)})\frac{a_{w(j)}P^o_w}{P_T} + k_m(a_{w(j-1)} + a_{w(j+1)} - 2a_{w(j)}) \quad [1]$$

$$\lambda_{(j)} = 14.9a_{w(j)} - 44.7a^2_{w(j)} + 70a^3_{w(j)} - 26.5a^4_{w(j)} + 0.446a^5_{w(j)} \quad \text{mol water/mol } SO_3 \quad [2]$$

The total gas pressure is fixed and the local water activity in the membrane is assumed to be in equilibrium with the local gas phases, i.e., $a_{w(j)}P^o_w = P_{w(j)}$ and $P_{H2(j)} = P_{O2(j)} = P_T - P_{w(j)}$. The molar flow rates change along the flow channel as water is formed and reactants are consumed; the molar flows are given by $F_{A(j)} = F_{A(j-1)} - i_{(j)}/4F$ and $F_{C(j)} = F_{C(j-1)}$. Finally, we assume the local potential between the anode and cathode is the thermodynamic potential as given in Eq. 3, where P^o is the standard state pressure (1 bar) for hydrogen and oxygen. (The thermodynamic potential assumption neglects interfacial potential drops due to finite reaction rates, resulting in the predicted currents being about 20% larger than those found in real fuel cells.)

$$V_{FC(j)} = 1.23 + \frac{RT}{4F}\ln\left[\frac{\left(P_{H2(j)}/P^o\right)^2\left(P_{O2(j)}/P^o\right)}{(a_{w(j)})^2}\right] \text{ Volt} \quad [3]$$

Based on the equivalent electrical circuit, the differential elements that are in series for gas flow are electrically connected in parallel to each other. The voltage across the external load resistance thus depends on the total current produced by all elements; the local current is given by Eq. 4. The local membrane resistance, $R_{M(j)}$, depends on the local water content in the membrane and the area of the differential element; the area of the membrane element was taken to be one-sixth the total membrane area of total MEA area of 1.2 cm^2. For a Nafion 115 membrane employed in the SAPC fuel cell the membrane resistance as a function of water activity is given by Eq. 5

$$i_{(j)} = \frac{V_{FC}(j) - R_L\sum_{k\neq j} i_{(k)}}{R_L + R_{M(j)}} \quad [4]$$

$$R_{M(j)} = \frac{\{5\times 10^5 \exp(-14a^{0.2}_{w(j)})\Omega - \text{cm}^2\}}{\{\text{membrane area}\}/6} \quad [5]$$

Ignition occurs when the local production of water in the fuel cell exceeds the water removed by convection. Water production depends on the load resistance and the membrane resistance. A dry membrane has a resistance of 500 kΩ-cm^2, limiting the current density to a maximum of 2.4 μA/cm^2 ($j = 1.2$ V/R); at 80°C the feed flow rates would have to be $<10^{-3}$ cm^3/min to ignite the fuel cell. Absorption of 10 μL/cm^2, of water into the membrane reduces its resistance to $\sim$10 Ω-cm^2, increasing the maximum current density to 100 mA/cm^2. For gas flow rates of <10 cm^3/min, this current is sufficient for the fuel cell current to ignite at temperatures $\leq$50°C, as shown in Fig. 2.

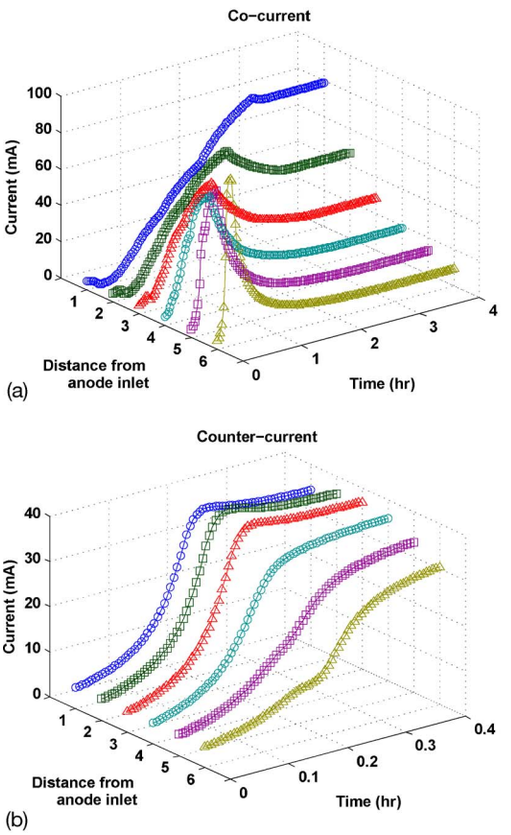

Figure 11. (Color online) Simple model fit to the current ignition and front propagation in the segmented anode parallel channel fuel cell. The model gives a good semiquantitative account of current ignition. (a) Co-current flow. (b) Counter-current flow. Simulated conditions: 5 sccm feed flow rates of H_2 at both anode and O_2 at the cathode, 50°C, 5 Ω load resistance.

The key elements that account for ignition are an exponential increase of proton conductivity in the PEM with membrane water content and the dynamics of water uptake into the PEM. The location of ignition and front propagation are consequences of convection of water produced downstream where it can accumulate and diffusion of water upstream through the polymer membrane. The simple model can capture the current ignition and current front propagation, though the model predicts larger currents than we observed experimentally. Figure 11 shows the model prediction of the ignition front propagation for co-current and counter-current flows and can be compared to the experimental data shown in Fig. 7. The time scales are approximately correct and the current densities are within 25% of the experimental values. The performance of this simple model is satisfactory.

The model is only semiquantitative; it neglects finite mass transfer rates of water into the membrane and from the membrane into the gas phase at the anode and cathode. The model also neglects the effects of liquid water on hindering gas transport from the flow channels to the membrane/electrode interface. More complex models that incorporate these effects can give quantitative fits to the experimental results, but do not alter the basic physics.

For co-current flow, the water produced upstream is conducted toward the outlet, where it slowly accumulates in the membrane. When the water content increases to the point where the local membrane resistance becomes comparable to the external load resistance the current increases rapidly, hydrating the membrane and causing ignition at the outlet of the flow channel. Water is also transported upstream through diffusion in the membrane itself, causing upstream propagation of the current ignition. The model did not capture the decreases in the downstream current after the ignition propagated to the inlet of the fuel cell. We attribute the decrease in downstream proton current after ignition to liquid water accumulating in the cathode, inhibiting oxygen transfer to the catalyst and reducing the current. A more complicated model that includes two phase flow of water liquid and vapor would be necessary to simulate these phenomena.

The two stage ignition with a current pulse at short times when the reactants first arrived at the membrane/electrode interface was not captured in the model. There are other complexities in the experiment that the model does not capture. The rise in current in the downstream segments before extinction, and the negative currents in the central segments are not predicted at all by the model. These phenomena result from electrical communication between segments that we ignored. For example, the negative currents shown in the extinction data in Fig. 3 suggest that there are potential differences between segments 4, 5, and 6 that drive local currents where hydrogen is oxidized at the electrode on segments 5 and 6, and the protons move through the membrane to segment 4 where they are reduced to hydrogen.

Liquid water was observed leaving the flow channels 30–40 min after ignition. Ignition takes the fuel cell from very low water activity to water activity close to unity, followed by accumulation of water and, eventually, condensation of liquid water in the flow channels. Gravity plays a key role in how such liquid water moves through the flow channels; the operation changes dramatically if gas flow in the channel is counter to gravity driven liquid water flow. When the fuel cell was vertical, gravity caused the liquid to drain and permitted good access for the reactants from the flow channels to the electrode/electrolyte interface. We observed that when the fuel cell was positioned so that liquid water could freely drain under gravity, the steady state fuel cell operation was stable. However, when the fuel cell was oriented so that the gas flow needed to push liquid water against gravity, there were large fluctuations in the local current density, which appeared to show some correlation with water droplets exiting from the fuel cell. In the horizontal orientation, liquid water condensing in the flow channels could partially block flow, and this hindered the reactants from getting to the electrode/electrolyte interface. The liquid drops were pushed along the flow channels by the flowing gas, but in an irregular fashion, that gave rise to large fluctuations in the local current density. Transport of liquid water in the flow channels is not accounted for at our level of modeling. We examined many published models for PEM fuel cells and we found none that considered the effects of gravity on the two phase flow in PEM fuel cells.[1,3,10,12,22,32,40-44] The role of gravity on two-phase flow in PEM fuel cells could play an essential role in the control for PEM fuel cells systems.

Conclusions

Current ignition in PEM fuel cells is analogous to thermal ignition with exothermic reactions. The proton conductivity depends exponentially on the water content in the membrane, similar to the Arrhenius exponential dependence of the reaction rate constant on temperature. When the PEM fuel cell is operated autohumidified, current ignition results from a balance between water production and water removal; positive feedback between water produced and the proton conductivity in the polymer membrane ignites the current. Current ignition in the two dimensional gas flow channel gives rise to spatio-temporal current density fronts that propagate. The current density fronts are analogous to flame fronts, but result from nonlinear dynamics due to water concentration.

We introduced a model fuel cell reactor with a segmented anode and parallel flow channels. This model reactor permitted the measurement of local currents along the length of the flow channel. Current ignition and extinction were followed as functions of reactor temperature, feed flow rates, flow configuration, and load resistance. Co-current flow of the hydrogen at the anode and oxygen at the cathode ignited the current at the outlet from the flow channel; after ignition a current density front propagated toward the inlet due to water diffusion in the membrane. Counter-current hydrogen and oxygen flow resulted in current ignition toward the center of the flow channel with the current fanning out toward both ends. The key physical features of the ignition and front propagation can be captured with a relatively simple "tanks-in-series" model of the SAPC fuel cell reactor.

The orientation of the reactant gas flows relative to gravity plays a key role in the long-term stability of the fuel cell operation. When the reactant flows are assisted by gravity in draining liquid water from the flow channels, the currents are stable. When the fuel cell is oriented so the liquid water must be pushed from the flow channel by gas flow against gravity, the local current densities fluctuate. The current density fluctuations appear periodic, where the period is ~ 1 s for vertically oriented fuel cells and $\sim 10^4$ s for horizontally oriented fuel cells.

Acknowledgments

We thank the National Science Foundation (CTS-0354279 and DMR-0213707) for support of this work. J.E.C. and E.K. also thank the Princeton University Program in Plasma Science and Technology for partial support under U.S. Department of Energy contract no. DE-AC02-76-CHO-3073.

Princeton University assisted in meeting the publication costs of this article.

List of Symbols

$a_{w(j)}$	water activity in reactor element j
F	Faraday's constant (96,458 c/mol)
$F_{A(j)}$	molar flow rate in anode flow channel at differential element j
$F_{C(j)}$	molar flow rate in cathode flow channel at differential element j
$i_{(j)}$	current in reactor element j
k_m	mass transport coefficient for diffusive water transport between differential elements
N_{SO3}	sulfonic acid density (1.8×10^{-3}/cm^2)
P_w^o	water vapor pressure at reactor temperature T
$P_{O2(j)}$	partial pressure of oxygen in cathode flow channel element j
$P_{H2(j)}$	partial pressure of hydrogen in anode flow channel element j
$P_{w(j)}$	partial pressure of water in element j
P_T	total pressure in the gas flow channels
R	gas constant
R_L	external load resistance
$R_{M(j)}$	membrane resistance in element j
R_{sense}	sensing resistor for current measurements
T	fuel cell reactor temperature
V_A	volume of anode flow channel in a differential element of the reactor
V_C	volume of cathode flow channel in a differential element of the reactor
$V_{FC(j)}$	battery voltage in differential element j
$\lambda_{(j)}$	number of water molecules per sulfonic acid residue in the membrane

References

1. T. Thampan, S. Malhotra, J. X. Zhang, and R. Datta, *Catal. Today*, **67**, 15 (2001).
2. T. D. Gierke, G. E. Munn, and F. C. Wilson, *ACS Symp. Ser.*, **180**, 195 (1982).
3. A. Z. Weber and J. Newman, *Chem. Rev. (Washington, D.C.)*, **104**, 4679 (2004).
4. K. A. Mauritz and R. B. Moore, *Chem. Rev. (Washington, D.C.)*, **104**, 4535 (2004).
5. F. Barbir, *PEM Fuel Cells: Theory and Practice*, Elsevier Academic Press, Burlington, MA (2005).
6. *Fuel Cell Systems*, L. Blomen and M. Mugerwa, Editors, Plenum, New York (1993).
7. R. O'Hayre and F. B. Prinz, *J. Electrochem. Soc.*, **151**, A756 (2004).
8. J. Larminie and A. Dicks, *Fuel Cell Systems Explained*, 2nd ed., Wiley, New York (2003).
9. http://www.ballard.com/be_a_customer/transportation/fuel_cell_modules/mark_902#

10. C. Y. Wang, *Chem. Rev. (Washington, D.C.)*, **104**, 4727 (2004).
11. D. M. Bernardi and M. W. Verbrugge, *AIChE J.*, **37**, 1151 (1991).
12. D. M. Bernardi and M. W. Verbrugge, *J. Electrochem. Soc.*, **139**, 2477 (1992).
13. D. Natarajan and T. A. Van Nguyen, *J. Electrochem. Soc.*, **148**, A1324 (2001).
14. A. Su, Y. C. Chiu, and F. B. Weng, *Int. J. Energy Res.*, **29**, 409 (2005).
15. S. Dutta, S. Shimpalee, and J. W. Van Zee, *Int. J. Heat Mass Transfer*, **44**, 2029 (2001).
16. S. Shimpalee, S. Greenway, D. Spuckler, and J. W. Van Zee, *J. Power Sources*, **135**, 79 (2004).
17. J. Benziger, E. Chia, E. Karnas, J. Moxley, C. Teuscher, and I. G. Kevrekidis, *AIChE J.*, **50**, 1889 (2004).
18. J. Benziger, E. Chia, J. F. Moxley, and I. G. Kevrekidis, *Chem. Eng. Sci.*, **60**, 1743 (2005).
19. H. A. Gasteiger and M. F. Mathias, Paper presented at *Advances in Materials for Proton Exchange Membrane Fuel Cell Systems*, ACS, Feb 23–27, 2003.
20. *Fuel Cell Handbook*, U.S. Department of Energy, Morgantown, WV (2000).
21. *Handbook of Fuel Cells*, W. Vielstich, A. Lamb, and H. Gasteiger, Editors, Wiley, New York (2003).
22. W. K. Lee, S. Shimpalee, and J. W. Van Zee, *J. Electrochem. Soc.*, **150**, A341 (2003).
23. I. D. Raistrick, U.S. Pat. 4,876,115 (1989).
24. J. F. Moxley, S. Tulyani, and J. B. Benziger, *Chem. Eng. Sci.*, **58**, 4705 (2003).
25. W. H. J. Hogarth and J. B. Benziger, *J. Electrochem. Soc.*, **153**, A2139 (2006).
26. F. N. Buchi and S. Srinivasan, *J. Electrochem. Soc.*, **144**, 2767 (1997).
27. W. H. J. Hogarth and J. B. Benziger, *J. Power Sources*, **159**, 968 (2006).
28. C. Yang, S. Srinivasan, A. B. Bocarsly, S. Tulyani, and J. B. Benziger, *J. Membr. Sci.*, **237**, 145 (2004).
29. H. S. Fogler, *Elements of Chemical Reaction Engineering*, Prentice Hall, Upper Saddle River, NJ (1999).
30. C. van Heerden, *Ind. Eng. Chem.*, **45**, 1242 (1953).
31. D. Luss, *Ind. Eng. Chem. Res.*, **36**, 2931 (1997).
32. S. Dutta, S. Shimpalee, and J. W. Van Zee, *J. Appl. Electrochem.*, **30**, 135 (2000).
33. I. Nazarov and K. Promislow, *Chem. Eng. Sci.*, **61**, 3198 (2006).
34. P. Berg, K. Promislow, J. St Pierre, J. Stumper, and B. Wetton, *J. Electrochem. Soc.*, **151**, A341 (2004).
35. P. Berg, K. Promislow, J. Stumper, and B. Wetton, *Chem. Eng. Sci.*, **2**, 111 (2005).
36. R. Bradean and A. Desousa, Paper 995, presented at the Meeting of The Electrochemical Society, Los Angeles, CA, Oct. 16–21, 2005.
37. K. H. Choi, D. H. Peck, C. S. Kim, D. R. Shin, and T. H. Lee, *J. Power Sources*, **86**, 197 (2000).
38. E. S. J. Chia, J. B. Benziger, and I. G. Kevrekidis, *AIChE J.*, **50**, 2320 (2004).
39. J.-S. Chia, I. G. Kevrekidis, and J. B. Benziger, *AIChE J.*, **52**, 3902 (2006).
40. T. Berning and N. Djilali, *J. Electrochem. Soc.*, **150**, A1589 (2003).
41. T. Berning, D. M. Lu, and N. Djilali, *J. Power Sources*, **106**, 284 (2002).
42. V. Gurau, L. Hongtan, and S. Kakac, *AIChE J.*, **44**, 2410 (1998).
43. I. M. Hsing and P. Futerko, *Chem. Eng. Sci.*, **55**, 4209 (2000).
44. D. Natarajan and T. Van Nguyen, *J. Power Sources*, **115**, 66 (2003).